

Higher-order Topological Mott Insulators

Koji Kudo¹, Tsuneya Yoshida^{1,2}, and Yasuhiro Hatsugai^{1,2}

¹Graduate School of Pure and Applied Sciences, University of Tsukuba, Tsukuba, Ibaraki 305-8571, Japan

²Department of Physics, University of Tsukuba, Tsukuba, Ibaraki 305-8571, Japan

(Dated: November 13, 2019)

We propose a new correlated topological state which we call a higher-order topological Mott insulator (HOTMI). This state exhibits a striking bulk-boundary correspondence due to electron correlations. Namely, the topological properties in the bulk, characterized by the \mathbb{Z}_3 spin-Berry phase, result in gapless corner modes emerging only in spin excitations (i.e., the single-particle excitations remain gapped around the corner). We demonstrate the emergence of the HOTMI in a Hubbard model on the kagome lattice, and elucidate how strong correlations change gapless corner modes at the noninteracting case.

Introduction.— The discovery of topological insulators/superconductors has opened a new field of study in condensed matter physics [1–5]. A remarkable phenomenon of these states is the bulk-edge correspondence [6, 7]; because of the topological properties in the d -dimensional bulk, gapless edge states emerge around $d - 1$ -dimensional boundaries of the system which result in the quantized electron-magnetic responses [1, 8] and the emergence of Majorana fermions [9–14]. So far impacts of correlation effects on topological states have been addressed as one of the significant issues of this field [15–21]. As the results of extensive studies, a variety of new phenomena have been reported which are induced by correlation effects on the gapless boundary states. For example, electron correlations may change the topological classification [22–35] which plays an important role for material searching. Furthermore, correlation effects induce the so-called topological Mott insulating state where systems show Mott physics only around the edges with maintaining nontrivial properties in the bulk [36–41].

Along with the above significant progress of correlated topological phases, new classes of topological insulators/superconductors have been proposed which are referred to as higher-order topological insulators/superconductors [42–50]. These phases exhibit the characteristic bulk-boundary correspondence; topological properties in the d -dimensional bulk predict gapless charge excitations around $d - 2$ - or $d - 3$ -dimensional boundaries, while gapless charge excitations are absent around $d - 1$ -dimensional boundaries. Recent theoretical and experimental studies elucidate that the above higher-order bulk-edge correspondence is ubiquitous phenomenon; it can be observed for a variety of materials [51–54]. For instance, hinge states are observed for a hexagonal pit on a bismuth (111) surface [51]. In addition, Majorana corner states are theoretically proposed for an ordinary two-dimensional topological insulator proximity to a cuprate superconductor [53].

The above recent progresses lead us the following crucial question: *what is the impact of electron correlations to higher-order topological phases?* Correlation effects of boundary modes have recently addressed based on a field

theory [55]. We would like to stress however that systematic analysis both for the bulk and boundaries may elucidate new topological states which is significant but still missing.

In this paper, we explore correlated systems from the above higher-order perspective. Our systematic analysis both for the bulk and boundaries discovers a novel topological state, a *higher-order topological Mott insulator* (HOTMI), which exhibits a novel bulk-boundary correspondence due to electron correlations. Namely, in contrast to the above mentioned higher-order topological insulators (HOTIs) for free-fermions, the topological properties in the d -dimensional bulk do not induce the gapless charge excitations. Instead, the bulk nontrivial properties result in gapless spin excitations around the $d - 2$ - or $d - 3$ -dimensional boundaries. Our analysis based on the exact diagonalization [56] verifies the emergence of HOTMIs in a Hubbard model on the kagome lattice. Specifically, our systematic numerical simulation elucidates that the system possesses topologically nontrivial properties characterized with the \mathbb{Z}_3 spin-Berry phase. Correspondingly, the system hosts gapless spin excitations around the corner while correlations effects destroy the gapless charge excitations. The above behaviors are also confirmed by analyzing an effective Hamiltonian for the strongly correlated limit.

Model and topological invariant.— Let us begin by describing our model and introducing the \mathbb{Z}_3 spin-Berry phase. We consider the system of spinful interacting electrons on the kagome lattice [57–65]. The Hamiltonian is given by $H = H_{\text{kin}}^{\Delta} + H_{\text{kin}}^{\nabla} + H_{\text{int}}$, with

$$H_{\text{kin}}^{\gamma} = t_{\gamma} \sum_{i,j \in \gamma} \sum_{\alpha, \beta = \uparrow, \downarrow} c_{i\alpha}^{\dagger} \sigma_{\alpha\beta}^z c_{j\beta} + \text{h.c.}, \quad (1a)$$

$$H_{\text{int}} = U \sum_i \left(n_{i\uparrow} - \frac{1}{2} \right) \left(n_{i\downarrow} - \frac{1}{2} \right). \quad (1b)$$

Here, $\gamma = \Delta$ or ∇ , $n_{i\alpha} = c_{i\alpha}^{\dagger} c_{i\alpha}$, $c_{i\alpha}^{\dagger}$ ($c_{i\alpha}$) is the creation (annihilation) operator on site i with spin $\alpha = \uparrow$ or \downarrow , and $i, j \in \Delta(\nabla)$ indicates the summation over the nearest-neighbor pairs $i < j$ belonging to upward (downward) triangles, see Fig. 1(a). We parametrize the hop-

ping parameters as $t_\Delta = t \sin \phi$ and $t_\nabla = t \cos \phi$ with $0 \leq \phi \leq \pi/2$, and suppose the relations $0 \leq U$ and $0 < t$. Since the phase of the hopping is spin-dependent due to the Pauli matrix σ^z in Eq. (1a), time-reversal symmetry is broken while the system preserves U(1) spin-rotational symmetry. In the following, we focus on the system at half-filling [66]. We note that the spin-dependent hoppings play an essential role in realizing the gapped phase for the half-filled noninteracting system. In Fig. 1(a), we show a sketch of the system with $N_{\text{UC}} = 10$ under the open boundary condition (OBC), where N_{UC} is the number of the unit cells.

To characterize the bulk topological properties, we introduce the spin-Berry phase that is the spin counterpart of the \mathbb{Z}_3 topological invariant [42, 67]. Firstly, we define the spin-Berry connection whose integral corresponds to \mathbb{Z}_3 spin-Berry phase. The spin-Berry connection is defined as $A_-(\vec{\theta}) = \langle G_-(\vec{\theta}) | dG_-(\vec{\theta}) \rangle$. Here, $|G_-(\vec{\theta})\rangle$ denotes the ground state of the modified Hamiltonian by a so-called local gauge twist which is defined as follows. We pick up a specific downward triangle, which includes the sites 1, 2, 3, and rewrite the Hamiltonian H_{kin}^∇ as $U_-(\vec{\theta}) H_{\text{kin}}^\nabla U_-^\dagger(\vec{\theta})$ with $\vec{\theta} := (\theta_1, \theta_2)$, $U_-(\vec{\theta}) = e^{in_1^- \theta_1} e^{-in_2^- \theta_2}$, and $n_j^- = n_{j\uparrow} - n_{j\downarrow}$. With the spin-Berry connection A_- , the \mathbb{Z}_3 spin-Berry phase is defined as $\gamma_- = \frac{1}{i} \int_C A_-$. Here, C represents the following path of the integral: $\vec{\theta} = \vec{f}(t)$ ($0 \leq t \leq 1$) with $\vec{f}(t) = 2\pi(t, t)$ for $0 \leq t < 1/3$ and $\vec{f}(t) = 2\pi(t, 1/2 - t/2)$ for $1/3 \leq t \leq 1$. To numerically compute the integral, we apply the method proposed in Ref. 68. This topological invariant is well-defined even if the system is interacting. The C_3 symmetry in the system brings its quantization as $\gamma_- = 2\pi n/3$ with $n = 0, 1, 2$.

Let us briefly review the behaviors of noninteracting case [42, 69]. For $U/t = 0$, our model provides three phases: (i) a HOTI phase with $\gamma_- = 2\pi/3$ for $0 \leq t_\Delta/t_\nabla < 1/2$, (ii) a metallic phase for $1/2 \leq t_\Delta/t_\nabla \leq 2$, and (iii) a trivial phase with $\gamma_- = 0$ for $2 < t_\Delta/t_\nabla < \infty$. The topological properties in the bulk for phase (i) result in gapless excitations for the single-particle spectrum around the corners. The average magnetization per unit cell is one-half in the gapped phases, (i) and (iii), which arises from the absence of time-reversal symmetry (for more details, see Sec. S1 of Supplemental Material [70]).

Overview of numerical results.— Before entering upon detailed discussions, let us overview our numerical results.

The interplay between correlation effects and the topological properties induces the HOTMI exhibiting a novel bulk-boundary correspondence. In contrast to the noninteracting case, the topological properties are not reflected in the single-particle excitations; introducing the Hubbard interaction destroys gapless excitations for the single-particle spectrum. Instead, the bulk-nontrivial properties result in the gapless spin excitations around

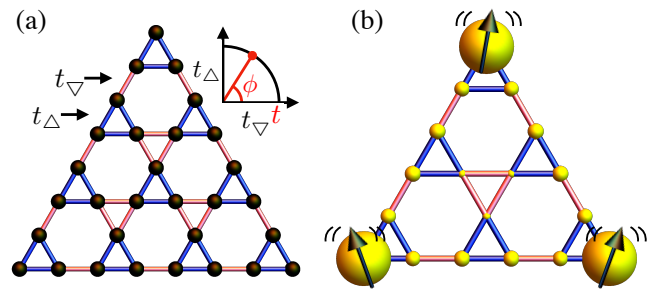


FIG. 1. (a) Sketch of the kagome lattice with $N_{\text{UC}} = 10$ and the boundary condition. Blue and red bonds represent nearest-neighbor hoppings corresponding to the Hamiltonian H_{kin}^Δ and H_{kin}^∇ , respectively. (b) $\langle \mathbf{S}_i^z \rangle - \langle \mathbf{S}_i^z \rangle_0$ computed by the Lanczos method for $N_{\text{UC}} = 6$, $t_\Delta/t_\nabla = 0.4$. In panel (b), the calculated value is represented by the radius of the spheres which is obtained under the OBC. The spin operator can be rewritten as $\mathbf{S}_i^z = 3(n_{i\uparrow} + n_{i\downarrow} - 2n_{i\uparrow}n_{i\downarrow})/4$.

the corners. Figure 1(b) supports the above behaviors. This figure shows the spin expectation value $\langle \mathbf{S}_i^z \rangle - \langle \mathbf{S}_i^z \rangle_0$ [71] at each site under the OBC for $t_\Delta/t_\nabla = 0.4$ and $N_{\text{UC}} = 6$. Here, $\langle \cdot \rangle$ and $\langle \cdot \rangle_0$ refer to the expectation values with respect to the ground state multiplet for $U/t = 1$ and $U/t = 0$, respectively. In Fig. 1(b), we can see that localized free-spins emerge only around the corners. This figure indicates the presence of gapless corner modes in the spin excitation spectrum due to the Mott behaviors occurring only around the corners.

In the following, we systematically analyze the system for the bulk and boundaries in order to verify the HOTMIs for the kagome Hubbard model.

Strong correlation limit.— As a first step, we analyze the kagome-Hubbard model in a strongly correlated limit $t/U \ll 1$. In this limit, electrons are completely localized in the entire system. However, we can still discuss the presence/absence of gapless spin excitations around the corners which are induced by the bulk-topological properties.

Based on the standard perturbation analysis for degenerated systems, we obtain the following effective spin model (see Sec. S2 of Supplemental Material [70]), $H_{\text{eff}} = H_\Delta^{(2)} + H_\nabla^{(2)} + H_\Delta^{(3)} + H_\nabla^{(3)}$, with

$$H_\gamma^{(2)} = J_\gamma^{(2)} \sum_{i,j,k \in \gamma} \left(-\frac{1}{2} \mathbf{S}_{ijk}^2 + S_{ijk}^z + \frac{3}{8} \right), \quad (2a)$$

$$H_\gamma^{(3)} = J_\gamma^{(3)} \sum_{i,j,k \in \gamma} S_{ijk}^z \left(-3\mathbf{S}_{ijk}^2 + 4S_{ijk}^z + \frac{9}{4} \right). \quad (2b)$$

Here, $J_\Delta^{(n)} = J^{(n)} \sin^n \phi$, $J_\nabla^{(n)} = J^{(n)} \cos^n \phi$, $J^{(n)} = 4t^n/U^{n-1}$, $\mathbf{S}_{ijk} = \mathbf{S}_i + \mathbf{S}_j + \mathbf{S}_k$ and $i, j, k \in \Delta(\nabla)$ indicates the summation over three sites $i < j < k$ composing upward (downward) triangles. $H_\gamma^{(2)}$ and $H_\gamma^{(3)}$ correspond to the second- and third-order-term, respectively. In the

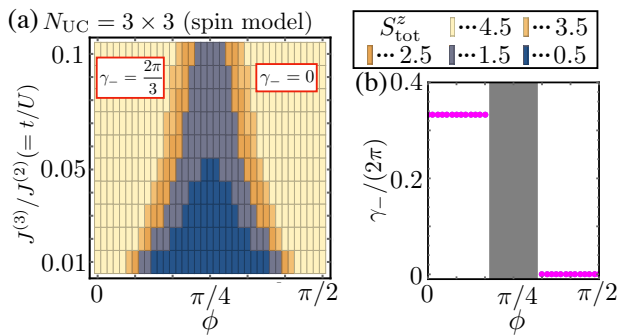


FIG. 2. Numerical results for the spin model (2). (a) S_{tot}^z of the ground state as a function of ϕ and $J^{(3)}/J^{(2)}$. (b) Spin-Berry phase γ_- of the ground state for $J^{(3)}/J^{(2)} = 0.1$ as a function of ϕ . The gray region in panel (b) indicates that S_{tot}^z of the ground state is not $N_{\text{UC}}/2 = 4.5$. The system is periodic and its size is $N_{\text{UC}} = 3 \times 3$ for panels (a) and (b).

absence of the third-order terms, the system is reduced to a spin system of the XXZ-interaction. The XXZ model preserves the time-reversal symmetry while the original Hamiltonian H does not. In order to remove the artificially produced symmetry, the third-order perturbation is necessary.

The presence of $H_\gamma^{(3)}$ is also essential for the bulk gap. To demonstrate it, let us analyze the cases for $\phi = 0$ or $\pi/2$ where the system is reduced to three-site problems under the periodic boundary condition (PBC). When the effective model includes only $H_\gamma^{(2)}$, the Kramers pair $|S_{123} = 3/2, S_{123}^z = \pm 1/2\rangle$ is realized as the ground state on three sites, which results in the macroscopic degeneracy in the bulk system. Introducing $H_\gamma^{(3)}$ breaks the time-reversal symmetry and lifts this Kramers degeneracy, which result in the unique ground state $|S_{123} = 3/2, S_{123}^z = 1/2\rangle$. This concise analysis suggests the emergence of the bulk gap even if the system is not completely decoupled ($0 < \phi < \pi/2$) unless the energy gap associated with the above three-site problem is vanishing. Figure 2(a) supports the presence of the bulk gap. In this figure, the ground state magnetization S_{tot}^z is plotted against ϕ and $J^{(3)}/J^{(2)} = t/U$. We remind that U(1) spin-rotational symmetry is preserved allowing us to label the energy eigenstates with S_{tot}^z . Figure 2(a) shows that the ground state with $S_{\text{tot}}^z/N_{\text{UC}} = 1/2$ extends to a finite range of ϕ , indicating that the energy gap observed for three-site problem remains finite. The energy eigenvalues as a function of ϕ is plotted in Sec. S3 of Supplemental Material [70] which directly supports the presence of the bulk gap.

Based on the result that the gap is finite in the region of $S_{\text{tot}}^z = 4.5$ [see Fig. 2(a)], let us discuss the topological properties of the ground state with $S_{\text{tot}}^z = N_{\text{UC}}/2$. Figure 2(b) plots its γ_- for $J^{(3)}/J^{(2)} = 0.1$ as a function of ϕ . The result indicates that the gapped phase for

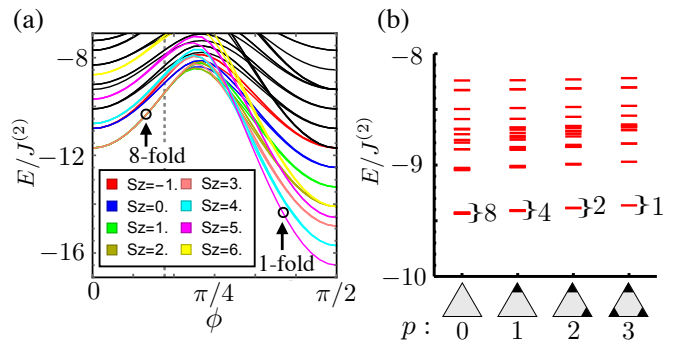


FIG. 3. Numerical results for the spin model (2). (a) Energy spectra $E/J^{(2)}$ as functions of ϕ . (b) Energy spectra $E/J^{(2)}$ at $\tan \phi = 0.5$ for each value of p , where p is the number of removed sites. Panels (a) and (b) are obtained for $N_{\text{UC}} = 10$ and $J^{(3)}/J^{(2)} = 0.1$ under the OBC. Only four lowest energies in the subspace specified by S_{tot}^z are shown here. The black lines in panel (a) express the energy for $S_{\text{tot}}^z < -1$ or $6 < S_{\text{tot}}^z$. The dashed line in panel (a) represents $\tan \phi = 0.5$.

$0 \leq \phi \lesssim \pi/4$ is characterized with $\gamma_- = 2\pi/3$ while the one for $\pi/4 \lesssim \phi \leq \pi/2$ is characterized with $\gamma_- = 0$. Because the gap remains finite in the yellow-colored regions in Fig. 2(a), we can characterize the topology of these gapped phases as summarized in this figure. We note here that the local gauge twist $U_-(\vec{\theta})H_{\text{kin}}^\nabla U_-^\dagger(\vec{\theta})$ defined in the Hubbard model is modified as $U_{\text{eff}}(\vec{\theta})(H_\nabla^{(2)} + H_\nabla^{(3)})U_{\text{eff}}^\dagger(\vec{\theta})$ for the effective model, where $U_{\text{eff}} = e^{2iS_1^z\theta_1}e^{-2iS_2^z\theta_2}$. The \mathbb{Z}_3 spin-Berry phase predicts to which decoupled limit ($\phi = 0, \pi/2$) a gapped phase is adiabatically connected.

So far, we have elucidated the topological properties in the bulk. In order to verify a novel bulk-boundary correspondence, we here analyze the systems under the OBC [Fig. 1(a)]. In a similar way as the previous case, we start with the cases of $\phi = 0$ and $\pi/2$ where the system is reduced to three-site problems. At $\phi = 0$, the coupling for upward triangle is zero ($H_\Delta^{(2)} = H_\Delta^{(3)} = 0$). Besides the trimer in the bulk, we can see the dimers for the one-dimensional edges due to the XXZ-spin interaction ($H_\nabla^{(2)}$). Furthermore, we can observe three free-spins on corners which are clearly gapless. These free-spins result in the eight-fold degeneracy of the ground state for the OBC. At $\phi = \pi/2$, the coupling for downward triangle is zero ($H_\nabla^{(2)} = H_\nabla^{(3)} = 0$). In this case, the system is composed only of trimers so that the ground state is unique and its S_{tot}^z is given as $S_{\text{tot}}^z = N_{\text{UC}}/2$.

To demonstrate the existence of this bulk-boundary correspondence at the other ϕ , we show in Fig. 3(a) the ϕ dependence of the energy $E/J^{(2)}$ for $J^{(3)}/J^{(2)} = 0.1$ under the OBC with $N_{\text{UC}} = 10$ [see, Fig. 1(a)]. For $0 \leq \phi \lesssim \pi/4$ ($\pi/4 \lesssim \phi \leq \pi/2$), the eight-fold degenerate (unique) ground state is observed. Their S_{tot}^z ranges between 0 and 3 (see Sec. S4 of Supplemental Material [70]).

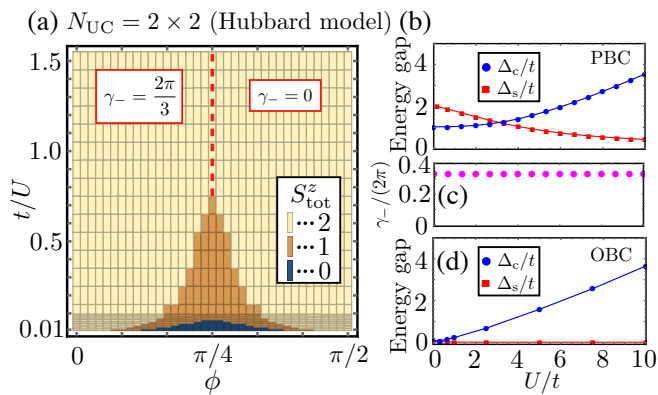


FIG. 4. Numerical results for the Hubbard model (1). (a) S_{tot}^z of the ground state as a function of ϕ and t/U . (b) Charge gap Δ_c and spin gap Δ_s as functions of U/t . (c) Spin-Berry phase γ_- as functions of U/t . (d) Charge gap Δ_c and spin gap Δ_s as functions of U/t . Panels (a), (b), and (c) are obtained for $N_{\text{UC}} = 2 \times 2$ under the PBC. Panel (d) is obtained for $N_{\text{UC}} = 6$ under the OBC. We set $t_{\Delta}/t_{\nabla} = 0.4$ in panels (b), (c), and (d).

To demonstrate that the 8-fold degeneracy is attributed to the gapless corner states, we remove a site located at each of ends (corners) and examine its effects on the degeneracy. Figure 3(b) plots the energy spectra for the four types of the geometry. Clearly, the ground state has 2^{3-p} -fold degeneracy corresponding to the defects of the p ends (corners), which suggests the emergence of the gapless modes at the $3-p$ corners for $0 \leq \phi \lesssim \pi/4$. Consequently, these results indicate that the HOTMI state emerges in the region with $\gamma_- = 2\pi/3$ shown in Fig. 2(a) which exhibits gapless corner states appearing only in spin excitations.

In the above, by analyzing the effective spin model, we have elucidated that the system exhibits the bulk-boundary correspondence of the HOTMI. Let us next analyze the Hubbard model beyond the framework of this effective theory.

From weakly to strongly correlated regions.— In response to the results of the effective spin model, two questions arise. “Does the HOTMI emerge in the Hubbard model even for the finite U/t ?” “If so, how the noninteracting HOTI state changes into the HOTMI state by electron correlations?” In the rest of this work, we address these issues by diagonalizing the Hamiltonian (1) and provide a numerical evidence that the HOTMI is exhibited in the system as long as $U/t \neq 0$.

Let us first investigate the bulk properties. In Fig. 4(a), we plot ground state magnetization S_{tot}^z for the PBC against ϕ and t/U in the same manner as the previous case. As for the region with $S_{\text{tot}}^z/N_{\text{UC}} = 1/2$ [i.e., the region with $S_{\text{tot}}^z = 2$ in Fig. 4(a)], it is suggested that the strongly and weakly correlated systems for $0 \leq \phi \lesssim \pi/4$ are adiabatically connected with

each other. Indeed, the energy gaps of the HOTI survives against the electron correlations. In Fig. 4(b), we show the U/t dependence of the charge and spin gaps for $t_{\Delta}/t_{\nabla} = 0.4$. Here, they are defined as $\Delta_c = (E_{\mathcal{N}_e+1, S_{\text{tot}}^z+1/2} + E_{\mathcal{N}_e-1, S_{\text{tot}}^z-1/2} - 2E_{\mathcal{N}_e, S_{\text{tot}}^z})/2$ and $\Delta_s = (E_{\mathcal{N}_e, S_{\text{tot}}^z+1} + E_{\mathcal{N}_e, S_{\text{tot}}^z-1} - 2E_{\mathcal{N}_e, S_{\text{tot}}^z})/2$, where \mathcal{N}_e and S_{tot}^z is the number of electrons and S_{tot}^z of the ground state, respectively [$\mathcal{N}_e = 3 \times N_{\text{UC}} = 12$ and $S_{\text{tot}}^z = 2$ in Fig. 4(b)]. Figure 4(b) indicates that Δ_c becomes of the order of U for large interactions, which clearly demonstrates that the HOTI for $U/t = 0$ is adiabatically connected into the HOTMI. Thus, they share the same topological character, which is indeed confirmed in Fig. 4(c), while they give the different bulk-boundary correspondence. In Fig. 4(a), there is no sign of the metallic behavior observed for the noninteracting case. This is due to a finite size effect, see Sec. S5 of Supplemental Material for more details [70].

Let us next analyze the system under the OBC, and show that the HOTI state expected to be transformed into the HOTMI state by the infinitesimal interaction for a sufficiently large system size. Figure 4(d) plots Δ_c and Δ_s with $N_{\text{UC}} = 6$ for $t_{\Delta}/t_{\nabla} = 0.4$ as functions of U/t . Here, the system gives the eight-fold degenerated ground state whose S_{tot}^z ranges between -1 and 2 (see Secs. S4 and S6 of Supplemental Material [70]) so that we set $\mathcal{N}_e = 18$ and $S_{\text{tot}}^z = 1$ to calculate the gaps Δ_c and Δ_s . Figure 4(d) implies that the gapless charge excitation is opened by the infinitesimal interaction U , which is consistent with the energy cost proportional to U induced by the double occupancy of a completely isolated site. On the other hand, the spin excitations remains gapless. We note that the behavior of Δ_c and Δ_s is associated with a kind of the Mott insulators with the finite charge gap and the zero spin gap exhibited at the corners. Thus, we call the gapless corner modes the novel bulk-boundary correspondence whose microscopic origin is the emergence of the corner-Mott states observed for $0 < U$. The bulk-boundary correspondence arising from electron correlations is precisely the defining feature of the HOTMI which is shown in Fig. 1(b).

Before closing, we note that the HOTMI state is considered to be ubiquitous. For example, the extension to other two-dimensional lattice models is expected to be possible. The formulation of the \mathbb{Z}_Q Berry phase for lattice models such as kagome and pyrochlore lattices [42] is recently generalized into any lattice model [72]; e.g. the \mathbb{Z}_4 Berry phase can be defined in the square lattice HOTI. By combining it with our approach, one expects that the square HOTI state [46, 72] would be transformed into the HOTMI state by the correlation effects. Furthermore, the HOTMI would be extended even to three-dimensions. This is because our approach can straightforwardly be applied to a system of the pyrochlore lattice, where its topology is characterized by \mathbb{Z}_4 spin-Berry phase [42]. In-

deed, our simple numerical calculations suggest that the correlation effect changes the pyrochlore HOTI state [69] into the HOTMI state, which will be discussed elsewhere in details.

Conclusion.— In this paper, we discovered a novel topological state, a HOTMI which exhibits a striking bulk-boundary correspondence. Namely, in contrast to higher-order topological insulators for free-fermions, the topology of d -dimensional HOTMIs results in the gapless $d-2$ - or $d-3$ -dimensional boundary states emerging only in the spin excitation spectrum; the single-particle spectrum remains gapped even around these boundaries. Our exact diagonalization analysis has verified the emergence of HOTMIs in the Hubbard model on the kagome lattice. Specifically, we have observed that the system possesses topological properties characterized by the spin-Berry phase with $\gamma_- = 2\pi/3$. We also observed that electron correlations open the charge gap around the corner, while the spin excitations remain gapless. These numerical results demonstrate the above novel bulk-boundary correspondence of HOTMIs.

We thank S. Hayashi, T. Mizoguchi, and H. Araki for fruitful comments. K. K. thanks the Supercomputer Center, the Institute for Solid State Physics, the University of Tokyo for the use of the facilities. The work is supported by JSPS KAKENHI Grant Numbers JP16K13845 (Y.H.), JP17H06138, JP18H05842 (T.Y.), and JP19J12317 (K.K.).

-
- [1] D. J. Thouless, M. Kohmoto, M. P. Nightingale, and M. den Nijs, *Phys. Rev. Lett.* **49**, 405 (1982).
- [2] C. L. Kane and E. J. Mele, *Phys. Rev. Lett.* **95**, 226801 (2005).
- [3] M. Z. Hasan and C. L. Kane, *Rev. Mod. Phys.* **82**, 3045 (2010).
- [4] X.-L. Qi and S.-C. Zhang, *Rev. Mod. Phys.* **83**, 1057 (2011).
- [5] M. König, S. Wiedmann, C. Brüne, A. Roth, H. Buhmann, L. W. Molenkamp, X.-L. Qi, and S.-C. Zhang, *Science* **318**, 766 (2007).
- [6] Y. Hatsugai, *Phys. Rev. Lett.* **71**, 3697 (1993).
- [7] Y. Hatsugai, *Phys. Rev. B* **48**, 11851 (1993).
- [8] X.-L. Qi, T. L. Hughes, and S.-C. Zhang, *Phys. Rev. B* **78**, 195424 (2008).
- [9] A. Y. Kitaev, *Physics-Uspokhi* **44**, 131 (2001).
- [10] J. Alicea, *Reports on Progress in Physics* **75**, 076501 (2012).
- [11] M. Sato and S. Fujimoto, *Journal of the Physical Society of Japan* **85**, 072001 (2016).
- [12] V. Mourik, K. Zuo, S. M. Frolov, S. R. Plissard, E. P. A. M. Bakkers, and L. P. Kouwenhoven, *Science* **336**, 1003 (2012).
- [13] L. P. Rokhinson, X. Liu, and J. K. Furdyna, *Nature Physics* **8**, 795 EP (2012).
- [14] A. Das, Y. Ronen, Y. Most, Y. Oreg, M. Heiblum, and H. Shtrikman, *Nature Physics* **8**, 887 EP (2012).
- [15] M. Hohenadler, T. C. Lang, and F. F. Assaad, *Phys. Rev. Lett.* **106**, 100403 (2011).
- [16] S.-L. Yu, X. C. Xie, and J.-X. Li, *Phys. Rev. Lett.* **107**, 010401 (2011).
- [17] T. Yoshida, S. Fujimoto, and N. Kawakami, *Phys. Rev. B* **85**, 125113 (2012).
- [18] Y. Tada, R. Peters, M. Oshikawa, A. Koga, N. Kawakami, and S. Fujimoto, *Phys. Rev. B* **85**, 165138 (2012).
- [19] T. Yoshida, R. Peters, S. Fujimoto, and N. Kawakami, *Phys. Rev. B* **87**, 085134 (2013).
- [20] M. Hohenadler and F. F. Assaad, *Journal of Physics: Condensed Matter* **25**, 143201 (2013).
- [21] S. Rachel, *Reports on Progress in Physics* **81**, 116501 (2018).
- [22] L. Fidkowski and A. Kitaev, *Phys. Rev. B* **81**, 134509 (2010).
- [23] L. Fidkowski and A. Kitaev, *Phys. Rev. B* **83**, 075103 (2011).
- [24] A. M. Turner, F. Pollmann, and E. Berg, *Phys. Rev. B* **83**, 075102 (2011).
- [25] Y.-M. Lu and A. Vishwanath, *Phys. Rev. B* **86**, 125119 (2012).
- [26] M. Levin and A. Stern, *Phys. Rev. B* **86**, 115131 (2012).
- [27] H. Yao and S. Ryu, *Phys. Rev. B* **88**, 064507 (2013).
- [28] S. Ryu and S.-C. Zhang, *Phys. Rev. B* **85**, 245132 (2012).
- [29] Y.-Z. You and C. Xu, *Phys. Rev. B* **90**, 245120 (2014).
- [30] H. Isobe and L. Fu, *Phys. Rev. B* **92**, 081304 (2015).
- [31] T. Yoshida and A. Furusaki, *Phys. Rev. B* **92**, 085114 (2015).
- [32] T. Morimoto, A. Furusaki, and C. Mudry, *Phys. Rev. B* **92**, 125104 (2015).
- [33] T. Yoshida and N. Kawakami, *Phys. Rev. B* **95**, 045127 (2017).
- [34] T. Yoshida, A. Daido, Y. Yanase, and N. Kawakami, *Phys. Rev. Lett.* **118**, 147001 (2017).
- [35] T. Yoshida, I. Danshita, R. Peters, and N. Kawakami, *Phys. Rev. Lett.* **121**, 025301 (2018).
- [36] D. Pesin and L. Balents, *Nature Physics* **6**, 376 EP (2010).
- [37] S. Rachel and K. Le Hur, *Phys. Rev. B* **82**, 075106 (2010).
- [38] T. Yoshida, R. Peters, S. Fujimoto, and N. Kawakami, *Phys. Rev. Lett.* **112**, 196404 (2014).
- [39] T. Yoshida and N. Kawakami, *Phys. Rev. B* **94**, 085149 (2016).
- [40] M. Kargarian and G. A. Fiete, *Phys. Rev. Lett.* **110**, 156403 (2013).
- [41] Topological Mott insulators discussed here differ from the interaction induced topological phase discussed in Ref. 73.
- [42] Y. Hatsugai and I. Maruyama, *EPL (Europhysics Letters)* **95**, 20003 (2011).
- [43] K. Hashimoto, X. Wu, and T. Kimura, *Phys. Rev. B* **95**, 165443 (2017).
- [44] W. A. Benalcazar, B. A. Bernevig, and T. L. Hughes, *Science* **357**, 61 (2017).
- [45] F. Schindler, A. M. Cook, M. G. Vergniory, Z. Wang, S. S. P. Parkin, B. A. Bernevig, and T. Neupert, *Science Advances* **4** (2018), 10.1126/sciadv.aat0346.
- [46] W. A. Benalcazar, B. A. Bernevig, and T. L. Hughes, *Phys. Rev. B* **96**, 245115 (2017).
- [47] S. Hayashi, *Communications in Mathematical Physics* **364**, 343 (2018).

- [48] S. Imhof, C. Berger, F. Bayer, J. Brehm, L. W. Molenkamp, T. Kiessling, F. Schindler, C. H. Lee, M. Greiter, T. Neupert, and R. Thomale, *Nature Physics* **14**, 925 (2018).
- [49] H. Araki, T. Mizoguchi, and Y. Hatsugai, *Phys. Rev. B* **99**, 085406 (2019).
- [50] S. A. A. Ghorashi, X. Hu, T. L. Hughes, and E. Rossi, *arXiv e-prints*, arXiv:1901.07579 (2019), arXiv:1901.07579 [cond-mat.mes-hall].
- [51] F. Schindler, Z. Wang, M. G. Vergniory, A. M. Cook, A. Murani, S. Sengupta, A. Y. Kasumov, R. Deblock, S. Jeon, I. Drozdov, H. Bouchiat, S. Guéron, A. Yazdani, B. A. Bernevig, and T. Neupert, *Nature Physics* **14**, 918 (2018).
- [52] M. Serra-Garcia, V. Peri, R. Süsstrunk, O. R. Bilal, T. Larsen, L. G. Villanueva, and S. D. Huber, *Nature* **555**, 342 EP (2018).
- [53] Z. Yan, F. Song, and Z. Wang, *Phys. Rev. Lett.* **121**, 096803 (2018).
- [54] C. Yue, Y. Xu, Z. Song, H. Weng, Y.-M. Lu, C. Fang, and X. Dai, *Nature Physics* (2019), 10.1038/s41567-019-0457-0.
- [55] Y. You, T. Devakul, F. J. Burnell, and T. Neupert, *Phys. Rev. B* **98**, 235102 (2018).
- [56] H. Q. Lin, *Phys. Rev. B* **42**, 6561 (1990).
- [57] Y. Imai, N. Kawakami, and H. Tsunetsugu, *Phys. Rev. B* **68**, 195103 (2003).
- [58] T. Ohashi, N. Kawakami, and H. Tsunetsugu, *Phys. Rev. Lett.* **97**, 066401 (2006).
- [59] M. Udagawa and Y. Motome, *Phys. Rev. Lett.* **104**, 106409 (2010).
- [60] Y. Furukawa, T. Ohashi, Y. Koyama, and N. Kawakami, *Phys. Rev. B* **82**, 161101 (2010).
- [61] A. Yamada, K. Seki, R. Eder, and Y. Ohta, *Phys. Rev. B* **83**, 195127 (2011).
- [62] S. Guertler, *Phys. Rev. B* **90**, 081105 (2014).
- [63] S. K. Kim and J. Zang, *Phys. Rev. B* **92**, 205106 (2015).
- [64] G. Chen and P. A. Lee, *Phys. Rev. B* **97**, 035124 (2018).
- [65] M. Nakamura and S. Nishimoto, *The European Physical Journal B* **91**, 203 (2018).
- [66] The model is also invariant under the transformation $c_{i\alpha}^\dagger \rightarrow \sigma_{\alpha\beta}^x c_{i\beta}$, which is a certain type of particle-hole symmetry.
- [67] T. Kawarabayashi, K. Ishii, and Y. Hatsugai, *Journal of the Physical Society of Japan* **88**, 045001 (2019).
- [68] T. Fukui, Y. Hatsugai, and H. Suzuki, *Journal of the Physical Society of Japan* **74**, 1674 (2005).
- [69] M. Ezawa, *Phys. Rev. Lett.* **120**, 026801 (2018).
- [70] See Supplemental Material, for details of bulk properties of the noninteracting HOTI, the derivation of the third-order perturbative Hamiltonian, the behavior of S_{tot}^z and additional numerical results for Figs. 2 (a) and 4, which includes Refs. 42 and 69.
- [71] H. Shiba and P. A. Pincus, *Phys. Rev. B* **5**, 1966 (1972).
- [72] H. Araki, T. Mizoguchi, and Y. Hatsugai, *arXiv e-prints*, arXiv:1906.00218 (2019), arXiv:1906.00218 [cond-mat.str-el].
- [73] S. Raghu, X.-L. Qi, C. Honerkamp, and S.-C. Zhang, *Phys. Rev. Lett.* **100**, 156401 (2008).

Supplemental Material

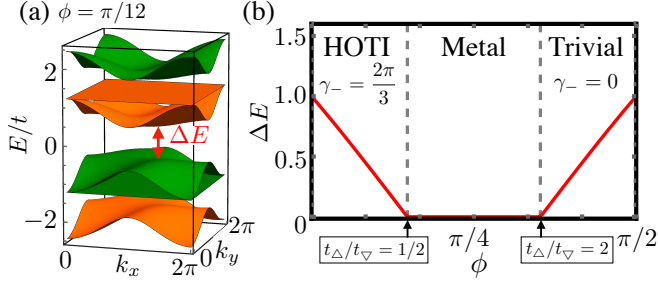


FIG. S1. (a) Band structure for $\phi = \pi/12$. The Green and orange bands represent $S_z = 1/2$ and $-1/2$, respectively. (b) Band gap ΔE between the third and fourth lowest bands as a function of ϕ . Gap closing points are indicated by dashed lines in panel (b).

S1. NONINTERACTING BULK PROPERTIES

In this appendix, we discuss the bulk properties of the noninteracting HOTI in our models. We note that the case of spinless fermion system has been studied in Refs. 42 and 69.

Let us start with investigating the band structure. Figure S1(a) shows the energy bands for $\phi = \pi/12$. Due to the $U(1)$ spin-rotational symmetry, we can label the bands with S_z . In Fig. S1(b), we plot the band gap ΔE between the third and fourth lowest bands as a function of ϕ . While the states for $1/2 \leq t_\Delta/t_\nabla \leq 2$ are gapless, the magnetic insulators are realized in both regions $t_\Delta/t_\nabla < 1/2$ and $2 < t_\Delta/t_\nabla$. The sum of S_z over the the three lowest bands is not vanishing so that the magnetization occurs. As formulated in Ref. 69, the system for $t_\Delta/t_\nabla < 1/2$ exhibits the HOTI phase that supports the gapless corner states under the OBC.

Next, we compute the spin-Berry phase γ_- in the two limits $\phi = 0$ and $\pi/2$. In the system at $\phi = 0$, the change of $\vec{\theta}$ is equivalent to the unitary transformation so that the Berry connection is given as

$$A_- = \langle G|U_-^\dagger dU_-|G\rangle = id\theta_1 \langle n_1^- | - id\theta_2 \langle n_2^- |. \quad (\text{S1})$$

Using $\langle n_1^- | = \langle n_2^- | = 1/3$, we have $\gamma_- = 2\pi/3$. On the other hand, γ_- for $\phi = \pi/2$ is vanishing due to the insensitivity of the Hamiltonian H_{kin}^Δ to $\vec{\theta}$. Because the gap is finite for $t_\Delta/t_\nabla < 1/2$ and $2 < t_\Delta/t_\nabla$, we can characterize the topology of these gapped phases as summarized in Fig. S1(b).

S2. THIRD-ORDER DEGENERATED PERTURBATION

In this appendix, we derive the effective Hamiltonian $H_\gamma^{(3)}$ in Eq. (2b) of the main text based on the degenerated perturbation theory. Let us first have a general

discussion. We consider a Hamiltonian $H_{\text{tot}} = H_0 + V$ with a perturbation V . If the ground state of the unperturbed problem (H_0 only) is degenerated and it is not lifted by the first-order and second-order perturbations, it is valid to diagonalize the effective Hamiltonian with the third-order perturbation given as

$$H_{\text{eff}}^{(3)} = PV\tilde{P}\frac{1}{(E^{(0)} - H_0)^2}\tilde{P}VPVP + PV\tilde{P}\frac{1}{E^{(0)} - H_0}\tilde{P}V\tilde{P}\frac{1}{E^{(0)} - H_0}\tilde{P}VP, \quad (\text{S2})$$

where P is the projection operator onto the degenerated ground state satisfying $H_0P = E^{(0)}P$, and $\tilde{P} = 1 - P$.

Let us then apply the above formulation to our model. When one sets $H_0 = H_{\text{int}}$ and $V = H_{\text{kin}}$, the projection operator P is given by the degenerated ground state where electrons are completely localized in the entire system. Since this projection operator satisfies $PH_{\text{int}}P = 0$ and $E^{(0)} = 0$, we get

$$H_{\text{eff}}^{(3)} = PH_{\text{kin}}\tilde{P}\frac{1}{H_{\text{int}}}\tilde{P}H_{\text{kin}}\tilde{P}\frac{1}{H_{\text{int}}}\tilde{P}H_{\text{kin}}P. \quad (\text{S3})$$

We note that there are three H_{kin} 's in Eq. (S3) so that the specific expression of Eq. (S3) is intrinsically given by solving the three-site problem.

To get the specific expression of Eq. (S3), we now consider the three-site problem and rewrite its Hamiltonian as

$$\mathcal{H} = \mathcal{H}_{\text{kin}} + \mathcal{H}_{\text{int}}, \quad (\text{S4a})$$

with

$$\mathcal{H}_{\text{kin}} = \sum_{i=1}^3 \sum_{\alpha=\uparrow,\downarrow} t_\alpha c_{i\alpha}^\dagger c_{i+1\alpha} + \text{h.c.}, \quad (\text{S4b})$$

$$\mathcal{H}_{\text{int}} = \sum_{i=1}^3 U n_{i\uparrow} n_{i\downarrow}. \quad (\text{S4c})$$

Here, $c_{4\alpha}^\dagger = c_{1\alpha}^\dagger$. The ground state multiplet in the unperturbed problem is given by

$$\Psi = (|\uparrow\uparrow\uparrow\rangle, |\uparrow\uparrow\downarrow\rangle, |\uparrow\downarrow\uparrow\rangle, |\downarrow\uparrow\uparrow\rangle, |\downarrow\downarrow\uparrow\rangle, |\downarrow\downarrow\downarrow\rangle, |\uparrow\downarrow\downarrow\rangle, |\downarrow\uparrow\downarrow\rangle), \quad (\text{S5})$$

where $|\alpha\beta\gamma\rangle = c_{1\alpha}^\dagger c_{2\beta}^\dagger c_{3\gamma}^\dagger |0\rangle$ and $|0\rangle$ is the vacuum state. The projection operators are given as $\mathcal{P} = \Psi\Psi^\dagger$ and $\tilde{\mathcal{P}} = 1 - \mathcal{P}$. Since $\mathcal{H}_{\text{kin}}|\uparrow\uparrow\uparrow\rangle = \mathcal{H}_{\text{kin}}|\downarrow\downarrow\downarrow\rangle = 0$, we focus on the sector of $S_{123}^z = \pm 1/2$, where $\mathbf{S}_{123} = \mathbf{S}_1 + \mathbf{S}_2 + \mathbf{S}_3$. As an example, one can show

$$\mathcal{H}_{\text{eff}}^{(3)}|\uparrow\uparrow\downarrow\rangle = \frac{1}{U^2} \{ 2(t_\downarrow^3 - t_\uparrow^3)|\uparrow\uparrow\downarrow\rangle + 3(t_\uparrow^2 t_\downarrow - t_\uparrow t_\downarrow^2)|\uparrow\downarrow\uparrow\rangle + 3(t_\uparrow^2 t_\downarrow - t_\uparrow t_\downarrow^2)|\downarrow\uparrow\uparrow\rangle \}, \quad (\text{S6})$$

where $\mathcal{H}_{\text{eff}}^{(3)}$ is the third-order perturbation in the three-site problem, see Eq. (S3). By using Eq. (S6), we get

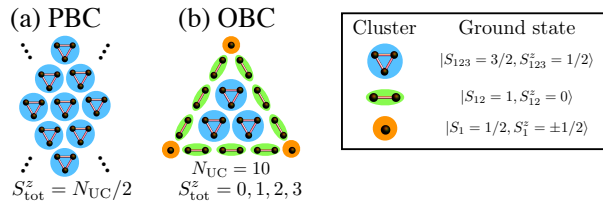


FIG. S3. Effective spin systems at $\phi = 0$ under (a) the PBC and (b) the OBC. The color expresses types of clusters.

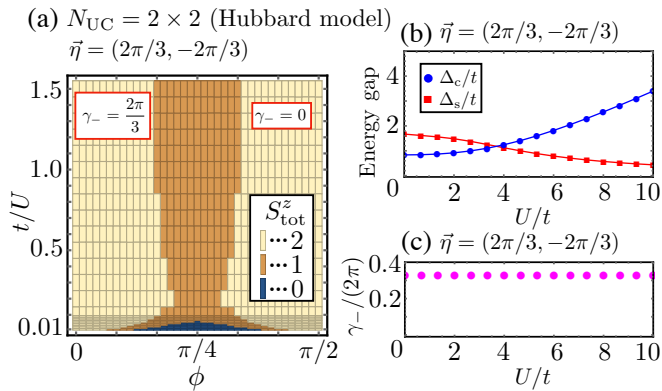


FIG. S4. The same as Figs. 4(a-c) in the main text but for $\vec{\eta} = (2\pi/3, -2\pi/3)$.

OBC is determined.

Let us first focus on the effective spin model for $N_{UC} = 10$ as discussed in Fig. 3(a). When setting $\phi = 0$, the system is reduced to three-site, two-site, and one-site problems shown in Fig. S3(b). The total S^z of ground state of each cluster is given as $S_{123}^z = 1/2$ (trimer), $S_{12}^z = 0$ (dimer) and $S_1^z = \pm 1/2$ (isolated site), respectively. Therefore, the whole system gives the eight-fold degenerated ground state whose S_{tot}^z ranges between 0 and 3, which is obtained by the straightforward calculation $(1/2) \times 3 + 0 \times 9 + (\pm 1/2) \times 3$ [see Fig. S3(b)]. This is consistent with the results in Fig. 3(a) at $\phi = 0$.

The total S^z of ground states of the cluster for the Hubbard model is same as that of the spin model. For example, the system for $N_{UC} = 6$ as discussed in Fig. 4(b) but for $\phi = 0$ is composed of one trimer, six dimers and three isolated sites. They can be counted by considering the figure similar to Fig. S3(b) but for $N_{UC} = 6$. Then, the whole system gives the eight-fold degenerated ground state whose magnetization ranges between -1 and

2, which is obtained by the straightforward calculation $(1/2) \times 1 + 0 \times 6 + (\pm 1/2) \times 3$.

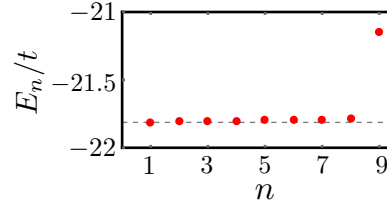


FIG. S5. Energy eigenvalues E_n/t . We set $U/t = 3$, $t_{\Delta}/t_{\nabla} = 0.4$, $N_{UC} = 6$ and $N_e = 3 \times N_{UC} = 18$. The dashed line represents the value of the lowest energy.

S5. WEAK CORRELATION REGIME AND FINITE SIZE EFFECT

In this appendix, we discuss the finite size effects on the results in Fig. 4(a). To investigate it, let us introduce the twisted boundary condition in both x and y directions. We generate Fig. S4(a) that is the same as Fig. 4(a) but for $\vec{\eta} = (2\pi/3, -2\pi/3)$, where $\vec{\eta} = (\eta_x, \eta_y)$ is the twisted angles. The figure clearly demonstrates the emergence of the region $S_{tot}^z = 1$ for the weak correlation regime, which does not exist in Fig. 4(a). This difference between the two figures suggests that the system size is too small to capture the metallic phase that is observed in the noninteracting system around $\phi \approx \pi/4$. On the other hand, the values of S_{tot}^z for $t_{\Delta}/t_{\nabla} \lesssim 1/2$ and $2 \lesssim t_{\Delta}/t_{\nabla}$ shown in both Fig. 4(a) and Fig. S4(a) are consistent with the result of the gapped noninteracting phases. To double check that the our conclusion in the main text is not dependent on $\vec{\eta}$, we here include Figs. S4(b) and (c) under $\vec{\eta} = (2\pi/3, -2\pi/3)$ that correspond to Figs. 4(b) and (c) in the main text. They clearly show the identical behavior.

S6. EIGHT-FOLD DEGENERACY FOR HUBBARD MODEL

In this appendix, we provide numerical evidences that the ground state of the Hubbard model under the OBC shows the eight-fold degeneracy as is the case of the effective spin model calculation in Fig. 3. In Fig. S5, we show the energy E_n/t for $U/t = 3$ and $t_{\Delta}/t_{\nabla} = 0.4$ under the OBC with $N_{UC} = 6$. It demonstrates the eight-fold degeneracy of the ground state, which implies the emergence of the corner-Mott states.